Supernova Shock Breakout from a Red Supergiant
Kevin Schawinski, *et al.*
Science **321**, 223 (2008);
DOI: 10.1126/science.1160456

14. C. A. B. Smith, *J. R. Stat. Soc. B* **15**, 153 (1953).
15. J. Bond *et al.*, *Nat. Genet.* **32**, 316 (2002).
16. X. Piao *et al.*, *Science* **303**, 2033 (2004).
17. T. Dixon-Salazar *et al.*, *Am. J. Hum. Genet.* **75**, 979 (2004).
18. I. Rudan, H. Campbell, A. D. Carothers, N. D. Hastie, A. F. Wright, *Nat. Genet.* **38**, 1224 (2006).
19. A. Mani *et al.*, *Proc. Natl. Acad. Sci. U.S.A.* **99**, 15054 (2002).
20. E. R. Ritvo *et al.*, *Am. J. Psychiatry* **142**, 187 (1985).
21. The Homozygosity Mapping Collaborative for Autism: Amman, Jordan: University of Jordan, Pediatrics, Najwa Khuri-Bulos, Amira Masri. Irbid, Jordan: King Abdullah University Hospital, Pediatrics and Child Neurology, Azhar Daoud. Jeddah, KSA: King Faisal Specialist Hospital and Research Centre, Pediatric Neurology, G.G.; Child Development and Pediatrics, S.B. Riyadh, KSA: King Faisal Specialist Hospital and Research Center, Genetics, Brian Meyer. Kuwait City, Kuwait: Kuwait Medical Genetics Centre, Sadika Al-Awadi; Kuwait Centre for Autism, S.A.-S. Muscat, Oman: Royal Hospital, Genetics Unit, Anna Rajab. Lahore, Pakistan: University of Health Sciences, A.H., in addition to Pakistan Psychiatric Research Centre, Haroon Rashid Chaudhry and Saima Niaz. Doha, Qatar: Weill Cornell Medical College in Qatar, Genetics and Pediatrics, Ahmad Teebi. Istanbul, Turkey: Istanbul University, Child Psychiatry, N.M.M., in addition to Sabri Herguner. Ankara, Turkey: SB Diskapi Children's Hospital, Ozgur Oner. Al Ain, UAE: United Arab Emirates University, Lihadh Al-Gazali, Valsamma Eapen. Dubai, UAE: Al Noor Centre for Children with Special Needs; Dubai Autism Center; Dubai Harvard Foundation for Medical Research, Muna Al Saffar. Sharjah, UAE: Manzil Centre for Challenged Individuals; Sharjah Autism Centre. Boston, MA, USA: C.A.W., E.M.M., S.Y.Y., R.S.H., J.N.P., B.B., R.M.J., J.W., in addition to Children's Hospital Boston, Developmental Medicine Center, Leonard Rappaport, Ramzi Nasir, Elaine LeClair, Ellen Hanson; Neurology, Annapurna Poduri; Clinical Genetics, Wen-Hann Tan; Massachusetts General Hospital, Pediatric Neurology, Ganeshwaran H. Mochida.
22. Materials and methods are available as supporting material on *Science* Online.
23. H. A. Hamamy, A. T. Masri, A. M. Al-Hadidy, K. M. Ajlouni, *Saudi Med. J.* **28**, 1015 (2007).
24. E. Hoodfar, A. S. Teebi, *J. Med. Genet.* **33**, 212 (1996).
25. L. G. Shaffer *et al.*, *J. Pediatr.* **149**, 98 (2006).
26. J. A. Vorstman *et al.*, *J. Am. Acad. Child Adolesc. Psychiatry* **45**, 1104 (2006).
27. International Molecular Genetic Study of Autism Consortium, *Am. J. Hum. Genet.* **69**, 570 (2001).
28. M. S. Takatalo, P. Kouvonen, G. Corthals, T. A. Nyman, R. H. Ronnholm, *Proteomics* **6**, 3502 (2006).
29. M. G. de Silva *et al.*, *J. Med. Genet.* **40**, 733 (2003).
30. S. H. Williamson *et al.*, *PLoS Genet.* **3**, e90 (2007).
31. M. Uemura, S. Nakao, S. T. Suzuki, M. Takeichi, S. Hirano, *Nat. Neurosci.* **10**, 1151 (2007).
32. Y. Yoshihara *et al.*, *Neuron* **13**, 415 (1994).
33. Y. Takano *et al.*, *J. Biol. Chem.* **279**, 18926 (2004).
34. A. E. West, E. C. Griffith, M. E. Greenberg, *Nat. Rev. Neurosci.* **3**, 921 (2002).
35. S. W. Flavell *et al.*, *Science* **311**, 1008 (2006).
36. G. A. Cox *et al.*, *Cell* **91**, 139 (1997).
37. G. D. Gilfillan *et al.*, *Am. J. Hum. Genet.* **82**, 1003 (2008).
38. W. Ji *et al.*, *Nat. Genet.* **40**, 592 (2008).
39. M. Alarcon *et al.*, *Am. J. Hum. Genet.* **82**, 150 (2008).
40. D. E. Arking *et al.*, *Am. J. Hum. Genet.* **82**, 160 (2008).
41. B. Bakkaloglu *et al.*, *Am. J. Hum. Genet.* **82**, 165 (2008).
42. C. L. Martin *et al.*, *Am. J. Med. Genet. B. Neuropsychiatr. Genet.* **144**, 869 (2007).
43. M. Park *et al.*, *Neuron* **52**, 817 (2006).
44. M. Sur, J. L. Rubenstein, *Science* **310**, 805 (2005).
45. C. Li, W. H. Wong, *Genome Biol.* **2**, 8 (2001).
46. We are grateful to the families who participated in this study. We also thank C. Lord for advice on phenotyping; D. Altshuler, M. Daly, and C. Lee for helpful discussions; C. Seidman, J. Seidman, and D. Housman for sharing control DNA; K. Allen, S. Tzakas, and C. Austin for technical assistance; and members of the Program in Medical and Populations Genetics at the Broad Institute, the Autism Consortium, and the Walsh laboratory for helpful discussions. We gratefully acknowledge the National Center for Research Resources Broad Institute Center for Genotyping and Analysis for expert design and execution of the SNP genotyping reported herein and the resources provided by the AGRE Consortium. AGRE is a program of Cure Autism Now (CAN) and is supported, in part, by grant MH64547 from the National Institute of Mental Health to Daniel H. Geschwind (PI). Genotyping services were also provided by the Center for Inherited Disease Research (CIDR). CIDR is fully funded through a federal contract from the National Institutes of Health to The Johns Hopkins University, contract number N01-HG-65403. We are grateful for support from CAN, the Nancy Lurie Marks Family Foundation, the Simons Foundation, the Harvard Kuwait Project, the Developmental Disabilities Research Center of Children's Hospital Boston (5P30HD018655-26), the Clinical Investigator Training Program of Harvard and Massachusetts Institute of Technology in collaboration with Pfizer Inc. and Merck & Co., the Anne and Paul Marcus Foundation, the Charles H. Hood Foundation, and NIH (1K23MH080954-01 to E.M.M, 1R01 MH083565 to C.A.W., 1K01MH71801 to R.J.F., and 5R01NS048276-05 to M.E.G.). E.M.M. holds a Career Award for Medical Scientists from the Burroughs Wellcome Fund and is also grateful for support from the Rappaport Research Scholarship in Neuroscience at Massachusetts General Hospital. S.-Y.Y. is a postdoctoral fellow of the National Alliance for Autism Research. M.E.G. is grateful for support from the F. M. Kirby Foundation. C.A.W. is an Investigator of the Howard Hughes Medical Institute.

Supporting Online Material

www.sciencemag.org/cgi/content/full/321/5886/218/DC1
Methods
Figs. S1 to S3
Tables S1 to S7
References

11 March 2008; accepted 12 May 2008
10.1126/science.1157657

REPORTS

Supernova Shock Breakout from a Red Supergiant

Kevin Schawinski,[1]* Stephen Justham,[1]* Christian Wolf,[1]* Philipp Podsiadlowski,[1] Mark Sullivan,[1] Katrien C. Steenbrugge,[2] Tony Bell,[1] Hermann-Josef Röser,[3] Emma S. Walker,[1] Pierre Astier,[4] Dave Balam,[5] Christophe Balland,[4] Ray Carlberg,[6] Alex Conley,[6] Dominique Fouchez,[7] Julien Guy,[4] Delphine Hardin,[4] Isobel Hook,[1] D. Andrew Howell,[6] Reynald Pain,[4] Kathy Perrett,[6] Chris Pritchet,[5] Nicolas Regnault,[4] Sukyoung K. Yi[8]

Massive stars undergo a violent death when the supply of nuclear fuel in their cores is exhausted, resulting in a catastrophic "core-collapse" supernova. Such events are usually only detected at least a few days after the star has exploded. Observations of the supernova SNLS-04D2dc with the Galaxy Evolution Explorer space telescope reveal a radiative precursor from the supernova shock before the shock reached the surface of the star and show the initial expansion of the star at the beginning of the explosion. Theoretical models of the ultraviolet light curve confirm that the progenitor was a red supergiant, as expected for this type of supernova. These observations provide a way to probe the physics of core-collapse supernovae and the internal structures of their progenitor stars.

The explosive deaths of massive stars are dramatic events that seed the Universe with heavy elements (*1*, *2*), produce black holes, pulsars, and the most energetic gamma-ray bursts (GRBs) (*3*). Their energy input can regulate the growth of galaxies (*4*). Even though a large amount of theoretical effort has been expended on trying to explain how the terminal collapse of a star's core leads to a luminous supernova, we do not fully understand the process by which the collapse of the core produces an outward-moving shock that leads to the ejection of the envelope (*5*–*7*). This shock heats and accelerates the stellar envelope as it passes through it. By the time the shock dissipates at the surface of the star, several solar masses of previously static envelope material are expanding at a few percent of the speed of light. At the time of core collapse, a nearby external observer equipped with a detector of neutrinos or of gravitational waves might receive a brief warning of the future explosion, but for most of the passage of the shock through the star, that observer would notice no further change. Only when the shock

[1]Department of Physics, University of Oxford, Oxford OX1 3RH, UK. [2]St John's College Research Centre, University of Oxford, Oxford OX1 3JP, UK. [3]Max-Planck-Institut für Astronomie, Königstuhl 17, 69117 Heidelberg, Germany. [4]Laboratoire de Physique Nucléaire et de Hautes Energies, CNRS-IN2P3 and Universités Paris VI and VII, 4 Place Jussieu, 75252 Paris Cedex 05, France. [5]Department of Physics and Astronomy, University of Victoria, Post Office Box 3055 STN CSC, Victoria, BC V8T 3P6, Canada. [6]Department of Physics and Astronomy, University of Toronto, 50 St. George Street, Toronto, ON M5S 3H4, Canada. [7]Centre de Physique des Particules de Marseille, CNRS-IN2P3 and Université Aix-Marseille II, Case 907, 13288 Marseille Cedex 9, France. [8]Department of Astronomy, Yonsei University, Seoul 120-749, Korea.

*To whom correspondence should be addressed. E-mail: kevins@astro.ox.ac.uk (K.S.), sjustham@astro.ox.ac.uk (S.J.), cwolf@astro.ox.ac.uk (C.W.)

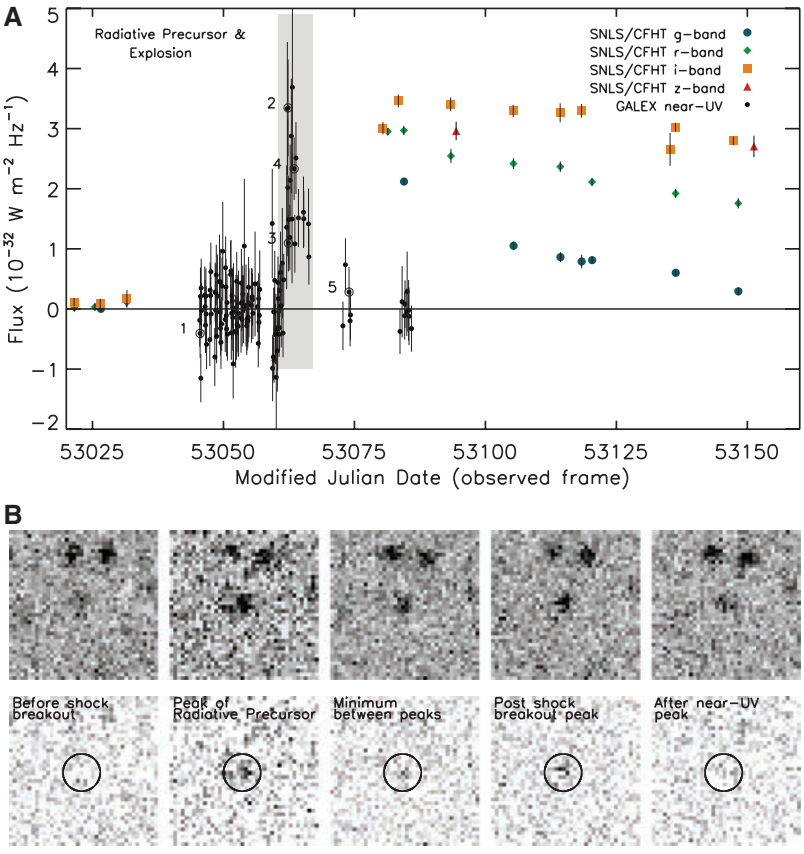

Fig. 1. (**A**) Composite of the optical SNLS and the UV GALEX light curves, or observed fluxes as a function of modified Julian date. All fluxes are host galaxy subtracted and are not corrected for internal extinction. The gray box indicates the time of the radiative precursor. The points highlighted by circles indicate five phases of the radiative precursor in the UV, as observed by GALEX. (**B**) These five phases are illustrated by a time sequence of original near-UV images (upper row, 1 × 1 arcmin) and difference images (lower row, with a pre-supernova image subtracted) to emphasize the transient source. Note the drop from point 2 to the minimum at 3 and the rise to 4, clearly visible in the GALEX images. The lack of optical data during the UV event is due to both poor weather conditions and technical problems. Both GALEX and SNLS light curves are available as tables in (*25*).

approaches the surface does radiation diffuse far enough ahead of the shock wave to raise the temperature of the stellar photosphere. This phase is sometimes referred to as "shock breakout," although the associated radiation is from the "radiative precursor" of the shock, long before the shock actually reaches the surface. This radiative precursor raises the temperature of the star to ~10^5 K before the surface expands dramatically (*8*).

Shock breakouts have been inferred for a few relatively local GRBs and x-ray flashes, which may involve shocks traveling through dense winds outside compact blue stars, including the recent SN 2008D (*9*–*14*). Here, we describe the brightening of a red supergiant due to the theoretically predicted radiative precursor before the supernova shock reaches the surface of the star. Such observations provide information about the density profile inside the progenitor star (*15*) and the physics of radiative shocks, and knowledge of the spectrum of the associated ultraviolet (UV) flash has implications for the ionization of the circumstellar medium (*16*, *17*).

Although core-collapse supernovae are expected to be most luminous around the time of shock breakout, most of this energy emerges as extreme UV or soft x-ray radiation. Hence, core-collapse supernovae are typically only discovered several days after the supernova explosion near the peak of their optical light curve; observations of early light curves are rare (*18*, *19*). To circumvent this problem, we exploit two complementary data sets: an optical survey to locate supernovae and UV data to search for serendipitously associated shock breakouts. The first is the Supernova Legacy Survey (SNLS) (*20*), which studies distant supernovae using data taken every 4 days at the 3.6-m Canada-France-

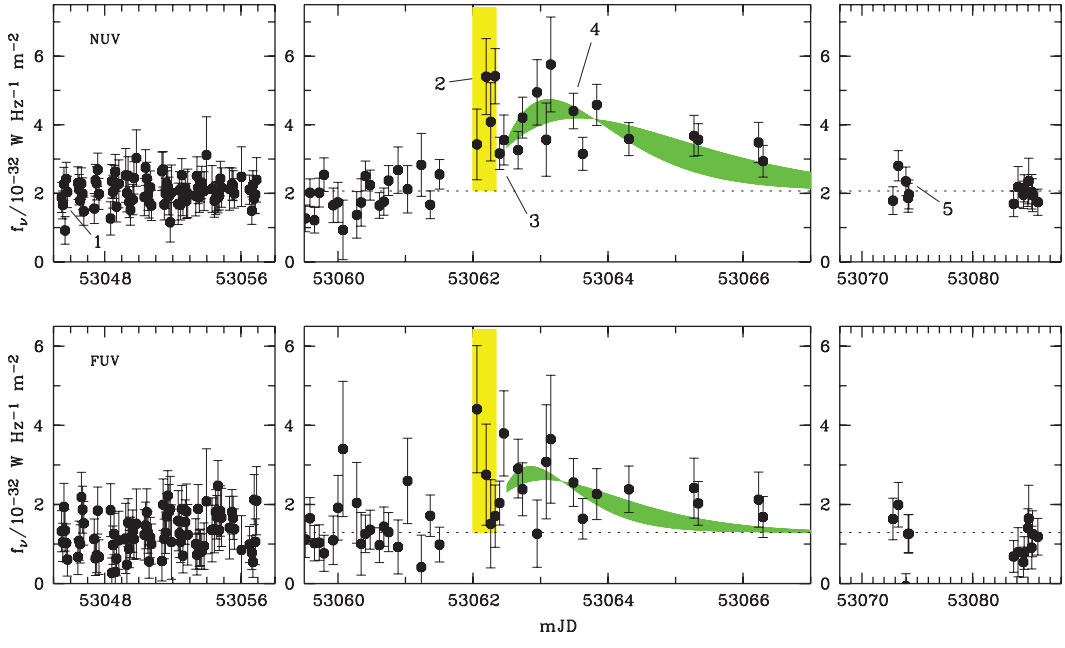

Fig. 2. The GALEX near-UV and far-UV flux against time (modified Julian date in days). This is a zoomed-in version of the shaded time range of Fig. 1 and we mark the same five data points. The background levels are shown before and after the supernova (left and right panels), and the central panels show the event itself. The radiative precursor is highlighted in yellow. Models for the post-explosion expansion are shaded in green; these models assume an initial photospheric radius of 500 to 1000 $R_\odot$. The width of the green band is due to the range of assumed expansion velocities (1 to 2 × 10^7 m s^{-1}). These models assume adiabatic free expansion of a radiation-dominated plasma and black-body emission from a well-defined photosphere. The models were only fitted to the near-UV data but are also consistent with the far-UV data.

Hawaii Telescope (CFHT). The second is from the Galaxy Evolution Explorer (GALEX) UV space telescope (*21*, *22*), which took a deep 100-hour combined exposure coincident with the early-2004 SNLS data in the Cosmological Evolution Survey (COSMOS) field (*23*, *24*). The Galaxy Evolution Explorer (GALEX) data were taken using subexposures of 15 to 30 min over several weeks, providing data with the time resolution necessary to resolve UV-luminous events occurring before the SNLS supernovae.

One SNLS event, designated SNLS-04D2dc and confirmed as a Type II supernova from the hydrogen lines in an optical spectrum taken at the European Southern Observatory (ESO) Very Large Telescope (VLT) [see supporting online material S1 (SOM text S1) (*25*)], shows a dramatic brightening in the GALEX near-UV images about 2 weeks before the discovery by the SNLS, consistent with shock breakout. The host galaxy appears to be a normal star-forming spiral galaxy at a redshift of $z = 0.1854$. The supernova spectrum, Gemini host galaxy spectrum, and Hubble Space Telescope image of the host are presented in (*25*). The optical light curve has a plateau that identifies the explosion as a Type IIP supernova (Fig. 1), suggesting a red-supergiant progenitor (*26*, *27*). Because of bad weather and technical problems with the CFHT camera, there are no optical data concurrent with the UV data; however, GALEX observed the entire radiative precursor (Fig. 2).

The GALEX light curve probes the arrival of the supernova shock at the surface of the star. We can interpret the two peaks in this light curve (Fig. 2) in terms of distinct physical processes. The first peak in the UV light curve is due to radiation traveling ahead of the shock wave. This heats the surface of the star before it begins to explode. The near-UV light curve samples the brightening caused by this precursor over ~6 hours. We can compare the duration of the observed precursor with theoretical expectations by equating the photon diffusion time scale with the time scale for the shock to escape from the envelope. If v is the shock speed and the density of the hydrogen-dominated atmosphere is ρ, we find $d \approx 2.5 \times 10^{11}$ m $(10^{-8}$ kg m$^{-3}/\rho)$ $(10^{7}$ m s$^{-1}/v)$ for the depth of the shock d (from the surface of the star) at the time when the radiative precursor becomes visible at the surface (SOM text 3 and 4). This value for d leads to a prediction for the duration of the shock precursor of $d/v = 2.5 \times 10^{4}$ s for the parameters above, that is, almost 7 hours, consistent with our observations of the precursor. This indicates that the progenitor was a large star, that is, a red supergiant, as expected for the progenitor of a type IIP supernova (*26*, *27*), whereas previous calculations indicated that radiative precursors from blue supergiant stars would last for minutes rather than hours (*8*). To model the radiative precursor, we solved simplified radiation-hydrodynamics equations for an outward-moving shock inside a stellar envelope. Figure 3 shows representative models that are consistent with the data; they require radii and envelope densities appropriate for a red-supergiant star. These models also indicate that only the initial ~4 hours of the first UV peak occur before the shock reaches the surface of the star.

The peak in the total luminosity of the source occurs at the time of the first UV peak, and the total luminosity monotonically decreases after this point. The temperature behind the shock is lower than the temperature at the shock front itself, which leads to a rapid drop in the luminosity of the star after shock breakout (*8*). The near-UV light curve in Fig. 3 shows this dip in brightness after the shock has escaped from the star.

Although the radiative precursor does cause some expansion of the star, there is little change in the stellar radius until the shock reaches the surface. Behind the shock, the radiation-dominated plasma expands at almost constant velocity and cools rapidly as a result of adiabatic expansion (*1*). The UV light curve is now governed by the expansion of the photospheric radius (and concomitant increase in radiating surface area), the adiabatic cooling of the surface, and the shift of the spectral energy distribution toward longer wavelengths, causing the second peak in the UV light curve. In the adiabatic cooling phase, the photospheric temperature T is approximately inversely proportional to the photospheric radius R. Because for a black body this drop in T causes a more rapid decrease in the luminosity ($L \propto T^4 \propto R^{-4}$) than the increase due to the growing surface area ($L \propto R^2$), the total luminosity of the supernova continues to decrease. However, in the Rayleigh-Jeans portion of the spectrum, the increase in the surface area of the photosphere is more important than the decrease in emission per unit area, and the luminosity at those wavelengths increases (SOM text S4.3). The observed UV luminosity rises until the peak of the black-body spectral energy distribution nears the UV waveband. Thereafter, the UV luminosity decreases with continued adiabatic expansion and cooling. The model curves in Fig. 2 show that this simple physical description reproduces the GALEX data with parameters as expected for a red supergiant progenitor. Initial photospheric radii of 500 to 1000 solar radii ($R_\odot$), expansion velocities of 1 to 2×10^7 m s^{-1}, and initial temperatures of ~10^5 K match the observed fluxes well. The biggest uncertainty arises from the adopted extinction (SOM text S1); any increase in the near-UV extinction would increase the range of preferred initial radii. Measuring precise radii of supernova progenitor stars would be a valuable constraint of the late stages in the evolution of massive stars; this requires higher time resolution and more accurate temperature determinations, for example, from observing the full spectral energy distribution from x-ray to optical. In addition, detailed light curves of radiative precursors probe the energetics of supernova shocks and the structures of the stellar envelopes through which they travel.

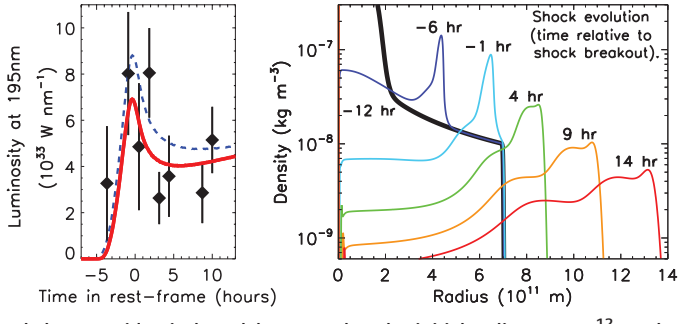

Fig. 3. (**Left**) Representative model precursor light curves compared with the precursor data (diamonds with error bars). The solid red curve represents the light curve produced from a model with an initial radius of 7×10^{11} m (≈1000 $R_\odot$) and an initial density distribution $\propto 1/r$. The dashed curve in the left panel shows an identical model, except that the initial radius was 10^{12} m; the absolute normalization of these luminosities is uncertain to factors of order unity (*25*). The zero point of the time axis is approximately at shock breakout. (**Right**) The time evolution of the internal density profile for the model producing the solid light curve in the left panel. About 4 hours before the shock has reached the surface, the UV luminosity has already begun to rise.

References and Notes

1. D. Arnett, *Supernovae and Nucleosynthesis: An Investigation of the History of Matter, from the Big Bang to the Present* (Princeton Series in Astrophysics, Princeton Univ. Press, Princeton, NJ, 1996).
2. K. Nomoto, N. Tominaga, H. Umeda, C. Kobayashi, K. Maeda, *Nucl. Phys. A.* **777**, 424 (2006).
3. C. L. Fryer *et al.*, *Publ. Astron. Soc. Pac.* **119**, 1211 (2007).
4. A. Dekel, J. Silk, *Astrophys. J.* **303**, 39 (1986).
5. R. Buras, M. Rampp, H.-T. Janka, K. Kifonidis, *Phys. Rev. Lett.* **90**, 241101 (2003).
6. A. Mezzacappa, *Annu. Rev. Nucl. Part. Sci.* **55**, 467 (2005).
7. A. Burrows, E. Livne, L. Dessart, C. D. Ott, J. Murphy, *Astrophys. J.* **640**, 878 (2006).
8. L. Ensman, A. Burrows, *Astrophys. J.* **393**, 742 (1992).
9. S. Campana *et al.*, *Nature* **442**, 1008 (2006).
10. A. M. Soderberg *et al.*, *Nature* **453**, 469 (2008).
11. P. A. Mazzali *et al.*, *Nature* **442**, 1018 (2006).
12. L.-X. Li, *Mon. Not. R. Astron. Soc.* **375**, 240 (2007).
13. G. Ghisellini, G. Ghirlanda, F. Tavecchio, *Mon. Not. R. Astron. Soc.* **382**, L77 (2007).
14. L.-X. Li, http://arxiv.org/abs/0803.0079 (2008).
15. A. J. Calzavara, C. D. Matzner, *Mon. Not. R. Astron. Soc.* **351**, 694 (2004).
16. C. Fransson, P. Lundqvist, *Astrophys. J.* **341**, L59 (1989).
17. P. Lundqvist, *Astrophys. J.* **511**, 389 (1999).
18. M. Stritzinger *et al.*, *Astron. J.* **124**, 2100 (2002).
19. R. M. Quimby *et al.*, *Astrophys. J.* **666**, 1093 (2007).
20. P. Astier *et al.*, *Astron. Astrophys.* **447**, 31 (2006).

21. D. C. Martin *et al.*, *Astrophys. J.* **619**, L1 (2005).
22. P. Morrissey *et al.*, *Astrophys. J. Supp. Ser.* **173**, 682 (2007).
23. N. Scoville *et al.*, *Astrophys. J. Supp. Ser.* **172**, 1 (2007).
24. M. A. Zamojski *et al.*, *Astrophys. J. Supp. Ser.* **172**, 468 (2007).
25. More details are available in the supporting material on *Science* Online.
26. S. W. Falk, W. D. Arnett, *Astrophys. J.* **180**, L65 (1973).
27. S. J. Smartt *et al.*, *Science* **303**, 499 (2004).
28. K.S. is supported by the Henry Skynner Junior Research Fellowship at Balliol College, Oxford. S.J. acknowledges support by the Science and Technology Facilities Council (STFC) and Global Jet Watch, C.W. and E.S.W. by STFC, and M.S. by the Royal Society. This work is supported by Acceleration and Basic research programs of Ministry of Science and Technology/Korean Science and Engineering Foundation to S.K.Y. We gratefully acknowledge use of data from the NASA GALEX satellite, the CFHT, the ESO VLT, the Gemini Observatory, and the Hubble Space Telescope.

Supporting Online Material
www.sciencemag.org/cgi/content/full/1160456/DC1
SOM Text
Figs. S1 to S4
Tables S1 to S4
References

13 May 2008; accepted 30 May 2008
Published online 12 June 2008;
10.1126/science.1160456
Include this information when citing this paper.

High-Efficiency Organic Solar Concentrators for Photovoltaics

Michael J. Currie,* Jonathan K. Mapel,* Timothy D. Heidel, Shalom Goffri, Marc A. Baldo†

The cost of photovoltaic power can be reduced with organic solar concentrators. These are planar waveguides with a thin-film organic coating on the face and inorganic solar cells attached to the edges. Light is absorbed by the coating and reemitted into waveguide modes for collection by the solar cells. We report single- and tandem-waveguide organic solar concentrators with quantum efficiencies exceeding 50% and projected power conversion efficiencies as high as 6.8%. The exploitation of near-field energy transfer, solid-state solvation, and phosphorescence enables 10-fold increases in the power obtained from photovoltaic cells, without the need for solar tracking.

Photovoltaic (PV) concentrators aim to increase the electrical power obtained from solar cells. Conventional solar concentrators track the Sun to generate high optical intensities, often by using large mobile mirrors that are expensive to deploy and maintain. Solar cells at the focal point of the mirrors must be cooled, and the entire assembly wastes space around the perimeter to avoid shadowing neighboring concentrators.

High optical concentration without excess heating in a stationary system can be achieved with a luminescent solar concentrator (LSC) (*1*–*5*). LSCs consist of a dye dispersed in a transparent waveguide. Incident light is absorbed by the dye and then reemitted into a waveguide mode. The energy difference between absorption and emission prevents reabsorption of light by the dye, isolating the concentrated photon population in the waveguide. In this way, LSCs can achieve high optical concentrations without solar tracking (*6*). Unfortunately, the performance of LSCs has been limited by self-absorption losses that restrict the maximum possible concentration factor. Here we describe an efficient variant of an LSC that mimics a four-level laser design and exhibits optical concentrations suitable for practical applications.

Typically, LSC dye molecules are cast into a transparent plastic sheet; however, we deposited a thin film of organic dye molecules onto glass. Our devices were fabricated with thermal evaporation, but solution processing could also be used. Precise control over the film composition allowed us to apply the recent advances of organic optoelectronics to LSCs, including Förster energy transfer (*7*), solid state solvation (*8*), and phosphorescence (*9*). We term the resulting devices organic solar concentrators (OSCs).

To obtain the highest power efficiencies, we constructed tandem OSCs (*2*). Incident solar radiation first encounters an OSC employing a short-wavelength dye. Longer wavelengths are transmitted through the first OSC and absorbed by a longer-wavelength dye in a second OSC (Fig. 1). Alternatively, solar radiation transmitted through the top OSC can be gathered by a bottom PV cell or used to heat water in a hybrid PV thermal system (*2*).

We quantify self-absorption losses in OSCs using the self-absorption ratio *S*, defined as the ratio of the absorption coefficients at the absorption and emission maxima. We examined two emissive dyes: 4-(dicyanomethylene)-2-*t-butyl*-6-(1,1,7,7-tetramethyljulolidyl-9-enyl)-4*H*-pyran (DCJTB) (*10*) and platinum tetraphenyltetrabenzoporphyrin [Pt(TPBP)] (*11*). As shown in Fig. 2A, *S* for a DCJTB-based OSC is ~80. DCJTB belongs to the dicyanomethylene (DCM) class of laser dyes and is characterized by large Stokes shifts and red emission with near-unity quantum efficiency. Batchelder *et al.* selected this class of dyes for solar-concentrator applications partly because of its high self-absorption ratio (*3*, *4*).

To reduce concentration quenching, DCJTB was doped (2% v/v) into the host material tris(8-hydroxyquinoline) aluminum (AlQ_3), which forms stable amorphous films. The resulting AlQ_3:DCJTB (2%) film was 5.7 μm thick with an absorbance of 1.1 absorbance units (au) at the DCJTB absorption peak. *S* is enhanced when AlQ_3 is used as the host. AlQ_3 provides a polar environment that stabilizes the highly polar DCJTB excited state. The effect is known as solid-state solvation, and it red-shifts the DCJTB photoluminescence (PL) (*8*).

Förster energy transfer was used to reduce the required concentration and hence the self-absorption of the emissive dye. For example, in the rubrene-based OSC of Fig. 2A, we used rubrene and DCJTB in a 30:1 ratio, the maximum possible without incurring significant concentration quenching in rubrene or incomplete Förster transfer to DCJTB. The resulting AlQ_3:rubrene (30%):DCJTB (1%) film was 1.6 μm thick with an absorbance of 1.2 au at the rubrene absorption peak. Förster energy transfer from rubrene to DCJTB increases the self-

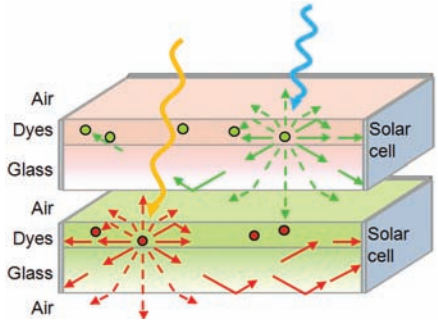

Fig. 1. Physical configuration of OSCs. (**Top**) OSCs consist of a thin film of organic dyes deposited on high-refractive-index glass substrates. The dyes absorb incident solar radiation and reemit it at a lower energy. Approximately 80% of the reemitted photons are trapped within the waveguide by total internal reflection for ultimate collection by a PV device mounted on the substrate edges. Photon loss (dashed lines) occurs because of nontrapped emission or absorption by other dyes. Blue arrow, high-energy incident visible light; green circles, dye molecules. (**Bottom**) Light transmitted through the first OSC can be captured and collected by a second OSC, whose dyes absorb and emit light at lower energies, for electrical conversion at a second, lower-bandgap PV device. Alternatively, the bottom OSC can be replaced by a low-cost PV cell or used to heat water in a hybrid PV thermal system. Yellow arrow, low-energy incident visible light; red circles, dye molecules.

Department of Electrical Engineering and Computer Science, Massachusetts Institute of Technology, Cambridge, MA 02139, USA.

*These authors contributed equally to this work.
†To whom correspondence should be addressed. E-mail: baldo@mit.edu